Information Sciences 273 (2014) 132–143

Contents lists available at ScienceDirect

Information Sciences

journal homepage: www.elsevier.com/locate/ins

Quaternion moment and its invariants for color object classification

Liqiang Guo [a,b,*], Ming Dai [b], Ming Zhu [b]

[a] School of Computer Science and Technology, Huaiyin Normal University, PR China
[b] Key laboratory of Airborne Optical Imaging and Measurement, Changchun Institute of Optics, Fine Mechanics and Physics, Chinese Academy of Sciences, PR China

ARTICLE INFO

Article history:
Received 2 September 2012
Received in revised form 7 March 2014
Accepted 11 March 2014
Available online 18 March 2014

Keywords:
Quaternion
Quaternion moment
Moment invariant
Pattern classification

ABSTRACT

Moment invariants are important shape descriptors in computer vision. In this study, we propose new sets of quaternion moment descriptors for color image. They are constructed in the quaternion framework and are an extension of complex moment invariants for grayscale images. This is a useful tool in color image processing and color object recognition tasks that require the similarity invariance. The advantage of the proposed quaternion moment invariants is that they can not only process color image in a holistic manner but also grayscale one. In addition, the computational complexity of the proposed method is much lower than the quaternion Zernike moments defined in the polar coordinates. An example of using the quaternion moment invariants as pattern features for a color object classification application is given. Theoretical and experimental results show that the proposed descriptors perform better than the other competing moment-based methods.

1. Introduction

Moment invariants have been become a useful tool for describing objects regardless of their position, viewing angle and illumination. Due to their ability to represent global features of an image, moment invariants have found widely applications in image processing and pattern recognition. The pioneering work of moment invariants was reported by Hu [17]. Since then, numerous works have been devoted to improvements Hu's moment invariants.

Teague proposed the Zernike and Legendre moments [51] by Zernike and Legendre polynomials, respectively. The definition of complex moments [26,27] were introduced by Abu-Mostafa and Psaltis, and gave us a straight forward way to derive moment invariants. Later, Fourier–Mellin descriptor was presented in [41,42] for image processing. Flusser et al. introduced the implicit moment invariants with respect to polynomial transform of spatial coordinates [10]. Besides, some excellent works have made outstanding contributions to the theory of moment invariants [9,28,53,54,13,5,24,32,55,35,48,20,44].

The moment invariants for grayscale images have been studied extensively, but little attention has been devoted to the corresponding theory for color images. Suk and Flusser derived a set of affine invariants based on geometric moments from different color channel [47]. Mindru et al. introduced the generalized color moments to processing color image and constructed the affine moment invariants [25].

In [15], we proposed the quaternion Fourier–Mellin moments (QFMMs), which can process the color image in a holistic manner. However, the QFMMs are defined in a polar coordinate system, whereas the images are expressed in a Cartesian one.

* Corresponding author at: School of Computer Science and Technology, Huaiyin Normal University, PR China. Tel.: +86 043186176563.
E-mail address: math_circuit@qq.com (L. Guo).

http://dx.doi.org/10.1016/j.ins.2014.03.037
0020-0255/

The transformations from one coordinate to another need to be done before we calculate the QFMMs. Besides, the coordinate conversion increases the computation complexity and affects the numerical stability.

Chen et al. proposed the Quaternion Zernike moments (QZMs) for color images, which are also defined in the polar coordinates [4]. They constructed a set of QZMs invariants with respect to similarity deformations. The QZMs have the virtue of the lower dependency among different orders. However, the calculation of Zernike polynomials was much more time-consuming, and then the computation complexity of the QZMs was much higher than the existing methods.

The objective of this paper is to introduce the quaternion-valued moments in Cartesian coordinate system for color image, and construct the similarity moment invariants. The advantage is obviously: first, the computation can be carried out directly and avoids the coordinate transformation; second, the computation complexity will be reduced.

The paper is organized as follows. In Section 2 we introduce the concept of quaternion moments for color images. Then, the construction of similarity invariants based on quaternion moments is investigated. Section 3 is the experimental results of the proposed invariants compared with other state-of-the-art alternatives in the aspect of color object classification. Section 4 concludes the paper.

2. Quaternion moment invariants

In this section we first give a brief introduction of the quaternion. Then we propose the concept of quaternion moments for color images. Last we construct the similarity invariants based on the proposed quaternion moments.

2.1. Quaternion

The quaternion, which is a type of hypercomplex numbers, was formally introduced by Hamilton in 1843. The definition of quaternion is

$$q = q_r + q_i i + q_j j + q_k k \tag{1}$$

where $q_r,\ q_i,\ q_j,\ q_k$ are real numbers and i, j, k are complex operators obeying the following rules

$$i^2 = j^2 = k^2 = -1,\ ij = -ji = k,\ jk = -kj = i,\ ki = -ik = j \tag{2}$$

A quaternion can be regarded as the composition of a scalar part and a vector part: $q = S(q) + V(q)$, where $S(q) = q_r,\ V(q) = q_i i + q_j j + q_k k$. If a quaternion q has a zero scalar part ($q_r = 0$), then q is called pure quaternion, and if q has a unit norm ($\|q\| = 1$), then q is called unit pure quaternion.

The norm of q is defined as

$$\|q\| = \sqrt{q_r^2 + q_i^2 + q_j^2 + q_k^2} \tag{3}$$

Euler's formula holds for quaternions, that is

$$e^{\mu\phi} = \cos(\phi) + \mu \cdot \sin(\phi) \tag{4}$$

where μ is any unit pure quaternion. We also have: $\|e^{\mu\phi}\| = 1$.

Sangwine proposed to encode the three channel components of a RGB image on the three imaginary parts of a pure quaternion [37], that is

$$f(x,y) = f_R(x,y)i + f_G(x,y)j + f_B(x,y)k \tag{5}$$

where $f_R(x,y),\ f_G(x,y)$ and $f_B(x,y)$ are the red, green and blue components of the pixel, respectively. In recent years, quaternion has been utilized more and more in color image processing domain [15,16,4,37–39,8,33,43,6,46,14]. The advantage of using quaternion to represent the color image is that we can process the image in a holistic manner without losing color information.

2.2. Quaternion moments

In this subsection we introduce the definition of quaternion moments. As Eq. (2) indicates, the commutative property for quaternion multiplication does not hold. Therefore the quaternion moment have three different types.

Definition 1. Let $f(x,y) = f_R(x,y)i + f_G(x,y)j + f_B(x,y)k$ represents the color image defined in Cartesian coordinate system, the $(m+n)$th order left-side quaternion moments of $f(x,y)$ are given by

$$Q_L[f(x,y)](m,n) = \int_{-\infty}^{\infty}\int_{-\infty}^{\infty}(x-\mu y)^m (x+\mu y)^n f(x,y)\,dx\,dy \tag{6}$$

the $(m+n)$th order right-side quaternion moments of $f(x,y)$ are given by

$$Q_R[f(x,y)](m,n) = \int_{-\infty}^{\infty}\int_{-\infty}^{\infty} f(x,y)(x-\mu y)^m (x+\mu y)^n\,dx\,dy \tag{7}$$

and the $(m+n)$th order two-side quaternion moments of $f(x,y)$ are given by

$$Q_T[f(x,y)](m,n) = \int_{-\infty}^{\infty}\int_{-\infty}^{\infty}(x-\mu y)^m f(x,y)(x+\mu y)^n dxdy \tag{8}$$

where m and n are positive integers, μ is any unit pure quaternion, for example: $\mu = i,\ \mu = j,\ \mu = k$, or $\mu = (i+j+k)/\sqrt{3}$, and so on.

If we set $\mu = i$, and $f(x,y)$ represents a real-valued function in Eqs. (6)–(8), then the proposed quaternion moments will be reduced to the complex moments. The advantage of quaternion moments is that it can not only process color image but also grayscale one.

In this paper, we will use left-side quaternion moments to construct the invariants, similar results can also be easily extended to the other two types of quaternion moments. From now on, and without loss of generality, we will assume that the quaternion moments refers to left-side one. We specify the unit pure quaternion as $\mu = (i+j+k)/\sqrt{3}$.

The discrete form of quaternion moments are given by

$$Q[f(x,y)](m,n) = \sum_{x=1}^{M}\sum_{y=1}^{N}(x-\mu y)^m (x+\mu y)^n f(x,y) \tag{9}$$

where M and N are the rows and columns of an image, respectively.

2.3. Quaternion moment similarity invariants

The similarity invariants of image moments are an important issue in pattern recognition. This subsection constructs the similarity invariants for color images based on quaternion moments.

The similarity transform of a color image consists of translation, rotation and uniform scale transforms. Let $f(x',y')$ is the transformed version of original image $f(x,y)$. We can use the following matrix equation to represent a similarity transform

$$\begin{pmatrix} x' \\ y' \end{pmatrix} = a\begin{pmatrix} \cos\varphi & -\sin\varphi \\ \sin\varphi & \cos\varphi \end{pmatrix}\begin{pmatrix} x \\ y \end{pmatrix} + \begin{pmatrix} \Delta x \\ \Delta y \end{pmatrix} \tag{10}$$

where a is scale factor with $a > 0$, φ is rotation angle, Δx and Δy are the translational components along x and y axes, respectively.

In the derivation of similarity invariants, we first represent the quaternion moments in polar coordinate through coordinate transformations

$$Q_L[f(r,\theta)](m,n) = \int_{r=0}^{\infty}\int_{\theta=0}^{2\pi} r^{m+n+1} e^{\mu(n-m)\theta} f(r,\theta) dr d\theta \tag{11}$$

where $f(r,\theta) = f_R(r,\theta)i + f_G(r,\theta)j + f_B(r,\theta)k$ represents a *RGB* color image defined in polar coordinates. The transformation process using the Euler's formula of quaternion (Eq. (4)) and following formulae

$$x = r\cos(\theta), \quad y = r\sin(\theta) \tag{12}$$

Let $f(r,\theta+\varphi)$ denotes the rotation change of a color image $f(r,\theta)$ by an angle φ, then quaternion moments (Eq. (11)) of $f(r,\theta+\varphi)$ and $f(r,\theta)$ have the following relations

$$\begin{aligned} Q_L[f(r,\theta+\varphi)](m,n) &= \int_{r=0}^{\infty}\int_{\theta=0}^{2\pi} r^{m+n+1} e^{\mu(n-m)\theta} f(r,\theta+\varphi) dr d\theta = e^{\mu(m-n)\varphi}\int_{r=0}^{\infty}\int_{\theta=0}^{2\pi} r^{m+n+1} e^{\mu(n-m)\theta} f(r,\theta) dr d\theta \\ &= e^{\mu(m-n)\varphi} Q_L[f(r,\theta)](m,n) \end{aligned} \tag{13}$$

Taking the norm on both sides of Eq. (13), we have

$$\|Q_L[f(r,\theta+\varphi)](m,n)\| = \left\|e^{\mu(m-n)\varphi}\ Q_L[f(r,\theta)](m,n)\right\| = \|Q_L[f(r,\theta)](m,n)\| \tag{14}$$

So, the rotation invariance can be achieved by taking the norm of the color images' quaternion moments. In other words, $\Phi_{m,n} = \|Q[\cdot](m,n)\|$ are invariant with respect to rotation transforms.

Suppose $f(ar,\theta)$ represents the color image expanded by the scale factor a, substitute $f(ar,\theta)$ into Eq. (11), then the following equation holds

$$\begin{aligned} Q_L[f(ar,\theta)](m,n) &= \int_{r=0}^{\infty}\int_{\theta=0}^{2\pi} r^{m+n+1} e^{\mu(n-m)\theta} f(ar,\theta) dr d\theta = a^{-(m+n+2)}\int_{r=0}^{\infty}\int_{\theta=0}^{2\pi} r^{m+n+1} e^{\mu(n-m)\theta} f(r,\theta) dr d\theta \\ &= a^{-(m+n+2)}\ Q_L[f(r,\theta)](m,n) \end{aligned} \tag{15}$$

Set $m = n = 0$ in Eq. (15), we have

$$Q_L[f(ar,\theta)](0,0) = a^{-2} Q_L[f(r,\theta)](0,0) \tag{16}$$

Divide Eq. (15) by Eq. (16), we have

$$\frac{Q_L[f(ar,\theta)](m,n)}{(Q_L[f(ar,\theta)](0,0))^{\frac{m+n+2}{2}}} = \frac{Q_L[f(r,\theta)](m,n)}{(Q_L[f(r,\theta)](0,0))^{\frac{m+n+2}{2}}} \tag{17}$$

Through Eq. (17), the scale factor a was eliminated. Therefore, the scale invariants can be constructed as follows

$$\Phi(m,n) = \frac{Q_L[f(r,\theta)](m,n)}{(Q_L[f(r,\theta)](0,0))^{\frac{m+n+2}{2}}} \tag{18}$$

We can also construct scale invariants as follows

$$\Phi(m,n) = \frac{Q_L[f(r,\theta)](m,n)}{(Q_L[f(r,\theta)](m,0))^{\frac{m+n+2}{m+2}}} \tag{19}$$

$$\Phi(m,n) = \frac{Q_L[f(r,\theta)](m,n)}{(Q_L[f(r,\theta)](0,n))^{\frac{m+n+2}{n+2}}} \tag{20}$$

We derived the rotation and scale invariants of quaternion moments by virtue of the polar coordinate. In other words, the rotation and scale parameters can be easily eliminated in polar coordinate. From Eq. (18), the rotation and scale moment invariants in Cartesian coordinates can be constructed as follows

$$\Phi(m,n) = \left\| \frac{Q_L[f(x,y)](m,n)}{(Q_L[f(x,y)](0,0))^{\frac{m+n+2}{2}}} \right\| \tag{21}$$

The translation invariance can be achieved by putting the origin of coordinates at the color image centroid. The centroid $(\bar{x},\bar{y})$ of a color image $f(x,y)$ are defined as follows

$$\bar{x} = \left\| \frac{\sum_{x=1}^{M}\sum_{y=1}^{N} x \cdot f(x,y)}{\sum_{x=1}^{M}\sum_{y=1}^{N} f(x,y)} \right\|, \quad \bar{y} = \left\| \frac{\sum_{x=1}^{M}\sum_{y=1}^{N} y \cdot f(x,y)}{\sum_{x=1}^{M}\sum_{y=1}^{N} f(x,y)} \right\| \tag{22}$$

In the computation of quaternion moment similarity invariants of a color image $f(x,y)$, we should first put the origin of Cartesian coordinates at the color image centroid, then calculate the similarity invariants using Eq. (21). The above derivation is also suitable for right-side and two-side quaternion moments.

Without loss of generality, the quaternion moment invariants (QMIs) are constructed by the left-side moments. In the appendix, we give an experimental result to validate the following fact: the discrimination power was almost unchanged whether the QMIs are constructed by left-side, right-side or two-side quaternion moments.

3. Experimental results and comparisons

In this section, experimental results are provided to validate the theoretical framework developed in the previous sections. The CMIs, QZMIs, QMIs are evaluated and compared in the context of color object classification.[1] We first demonstrate the performance of the proposed quaternion moment invariants by classifying the similarity transformed color objects. Then we test the robustness to different kinds of noises for the proposed descriptors. Next, we discuss the computation complexity of different kinds of invariant features. Last, we carried out an experiment on the classification of textured color images.

3.1. Testing and training data sets

The experiments are carried out on the selected thirty color images, as shown in Fig. 1, from the Columbia university image library database (Coil-100 color images) [30]. It is shown in Fig. 1 that (a1–a10) are the different types of car images, (b1–b10) are the different types of cup images and (c1–c10) are the different types of bottle images.

We use the color images shown in Fig. 1 to generate the testing image sets for color object classification experiments. To obtain the testing set, each car image in Fig. 1 (a1–a10) was translated with translation offsets $(\Delta x,\Delta y) \in \{(10,6),(2,12)\}$,[2] thus creating $10 \times 2 = 20$ samples. Then the above translated samples was rotated with rotation angle $\varphi \in \{k \cdot 30^\circ \mid k = 1,2,\ldots,11\}$, thus creating $10 \times 2 \times 11 = 220$ translated and rotated samples. Finally, scaled the above samples with scaling factors from 0.5 to 2 at an increment of 0.25, creating altogether $10 \times 2 \times 11 \times 7 = 1540$ samples as the final testing car image set.

To obtain the training set, we select 5 sample images in the testing set for different types of car images, then forming a set of $10 \times 5 = 50$ samples for the SVMs to get the training parameters. With this approach, we can obtain the testing and training image sets for the cup and bottle images in Fig. 1.

[1] There are many algorithms designed to serve this purpose, such as [36,18,45,1]. However, it is assumed that the background is uniform in our experiments. Thus, we have decided not to compare our proposals with local methods for color object classification.

[2] We can also use other translation parameters.

Fig. 1. Thirty images selected from the Coil-100 image database for color object classification. (a1–a10) are the different types of car images; (b1–b10) are the different types of cup images; and (c1–c10) are the different types of bottle images.

3.2. Support vector machines

In the past decade, support vector machines (SVMs) and related kernel methods have become one of the powerful tools to learn from examples with potential applications in computer vision and pattern recognition. The SVMs were proposed by Vlapnik [52], and were originally introduced within the context of statistical learning theory and structural risk minimization.

The central idea of SVMs is that they map the input vector nonlinearly into a higher dimensional feature space via a kernel function, and construct a optimal geometric hyperplane with the maximum margin to separates the data into classes. A detailed analysis of the SVMs is presented in [52,40,3]. In this paper, we use support vector machine with Gaussian RBF (radial basis function) kernel as classifier for color object classification.

The experiments in this section were carried out in the Matlab environment, and use the statistical pattern recognition toolbox for Matlab (abbreviated STPRtool) which was developed by Franc and Hlaváč [11]. The SVMs algorithm was achieved by using 'bsvm2', 'svmclass' and 'cerror' functions in the STPRtool.

The 'bsvm2' function trains the multi-class SVM classifier based on BSVM formulation (bias added to the objective function) and L2-soft margin penalization of misclassifications. The "options" parameters are set as follows: options.ker = 'rbf'; options.arg = 1; options.C = 10. The 'svmclass' function classifies input vectors into classes using the multi-class SVM classifier. The 'cerror' function Computes classification error. This function considers only labels, and the cross validation was not used in its. The detailed information can be found in the STPRtool [11].

3.3. Performance comparison of the proposed invariants with other invariants

The experimental results obtained by Chen et al. [4] indicated that quaternion Zernike moment invariants (QZMIs) perform better than some competing descriptors in the aspect of color object recognition. Those descriptors are traditional Zernike moment invariants, the affine invariants proposed by Suk and Flusser [47], the generalized affine color moment invariants [25], and the quaternion Fourier–Mellin moment invariants [15].

Due to a better performance of the QZMIs, we just give a comparison of the QZMIs with the proposed quaternion moment invariants (QMIs) in our experiments. Besides, the traditional complex moment invariants (CMIs) for grayscale image are also considered in the experiments to verify the importance of the color information for pattern recognition tasks. Note that in order to compress the data range, we perform the logarithm $\log_{10}(\cdot)$ on the CMIs, QZMIs and QMIs, separately.

In the following experiments, we demonstrate the effectiveness of the proposed invariant features in terms of color object classification.

3.3.1. Experiment on the noise-free image sets

The generic schematic diagram for the color object classification experiments using moment invariants and the SVMs is given in Fig. 2. First, the training process for the SVMs is performed. The complex moment invariants were computed on the training car images to form the CMIs descriptor set. Next, using the CMIs as the input vector and training the SVMs to get the related parameters such as the support vectors, weights and threshold. Then the CMIs descriptor set of the testing car images were computed, and classified the objects by the SVMs. Last, the above procedures were carried out for the QZMIs and the QMIs, respectively, to get the corresponding classification results. Similar procedures were implemented separately for the cup and bottle image sets.

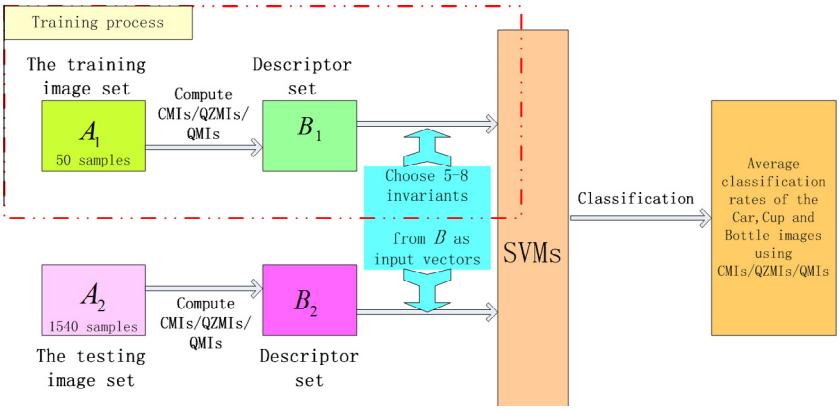

Fig. 2. Block diagram of the color object classification experiments. (For interpretation of the references to color in this figure legend, the reader is referred to the web version of this article.)

Table 1
Classification accuracies (%) of different moment invariants without noise.

Number of invariants	Average classification accuracy (%)								
	Car images			Cup images			Bottle images		
	CMIs	QZMIs	QMIs	CMIs	QZMIs	QMIs	CMIs	QZMIs	QMIs
5	43.42	81.32	83.90	65.14	92.37	97.15	47.08	88.83	91.54
6	45.49	85.69	89.48	66.89	95.69	98.46	48.15	92.71	95.14
7	47.93	87.57	92.70	68.64	96.92	98.82	48.81	95.08	96.78
8	50.97	87.79	93.77	70.91	97.27	100.00	50.06	96.56	97.53

The QZMIs descriptor set $\{|\bar{\varphi}^1_{1,1}|, |\bar{\varphi}^0_{2,0}|, |\bar{\varphi}^2_{2,2}|, |\bar{\varphi}^1_{3,1}|, |\bar{\varphi}^3_{3,3}|, |\bar{\varphi}^0_{4,0}|, |\bar{\varphi}^2_{4,2}|, |\bar{\varphi}^4_{4,4}|\}$ in our experiments, containing 8 invariants with order from 1 to 4, is selected from Table 1 of Ref. [4]. The QMIs descriptor set containing 8 invariants with order from 1 to 4: $\{\Phi(1,0), \Phi(0,1), \Phi(2,0), \Phi(0,2), \Phi(2,1), \Phi(3,0), \Phi(2,2), \Phi(3,1)\}$ is computed by Eq. (21). The CMIs descriptor set uses the same order as that of QMIs, also containing 8 invariants.

In our experiments, we use different numbers of moment invariants as the input vectors for the SVMs to validate the description power of the CMIs, QZMIs and QMIs. For example, we select 5 different invariants arbitrarily in the QMIs descriptor set as input vectors of the SVMs for color object classification. The input vectors can be selected as $\{\Phi(1,0), \Phi(0,1), \Phi(2,0), \Phi(0,2), \Phi(2,1)\}$ or $\{\Phi(0,2), \Phi(2,1), \Phi(3,0), \Phi(2,2), \Phi(3,1)\}$ and so on. Next we obtained a classification rates for each input vector and have $C(8,5) = 56$ results.[3] Then we compute the average classification rate in the condition of 5 invariants as color object descriptor for the testing car, cup and bottle image sets, separately. The similar procedure is performed using CMIs and QZMIs descriptor sets, separately, and gets the average classification rate for the corresponding image sets. The experimental results can be found in the first line of Table 1.

As we can see from the first line of Table 1, the quaternion-based moment invariants (QZMIs and QMIs) perform better than the CMIs no matter whether from the car, cup or bottle image set. The average classification rates using QZMIs and QMIs are much better than the CMIs. This is mainly caused by the graying process for the color image when computing the CMIs, where the color information can enhance the recognition rate. This is also validated by Tanaka and Presnell in Ref. [50] and Gepperth et al. in [12]. Besides, we can see that the description power of proposed moment invariants were better than the QZMIs.

The data in the second, third and fourth lines of Table 1 are, respectively, the average classification rate for different numbers of invariants from 6 to 8. The results indicate that the more invariants were selected, the higher classification rates were obtained. The above experiments on the noise-free image sets show that the proposed descriptors perform best in terms of the classification accuracy.

3.3.2. Experiment on the noised image sets

In the next two experiments, we investigate the robustness of the proposed QMIs to additive noise (Gaussian white noise and Salt and Pepper noise were used in our experiments). Fig. 3 demonstrate the corrupted image by different noise, where

[3] In this paper, the number of k-combinations from a given set of n elements is denoted by $C(n,k)$, and the number of $C(n,k)$ is computed by $C(n,k) = n!/(k!(n-k)!)$.

a1 is the original color image; a2 and a3 are the Gaussian noised color images of variance 0.01 and 0.03, respectively; a4 and a5 are the Salt and Pepper noised color images with noise density 0.03 and 0.05, respectively.

In the first experiment, the training and testing color image were corrupted by Gaussian noise with different variance (0.01 and 0.03). We validated the robustness against those noises for the proposed invariants by means of classification accuracy. The experimental results are listed in Tables 2 and 3.

As we can see from the above two tables, the classification accuracy of the noise corrupted images was lower than the noise-free one (compared with Table 1), and the classification accuracy decreases with the increase of noise. However, the proposed approach performs better than the CMIs and the QZMIs in terms of the classification accuracy.

The second experiment demonstrates the robustness of the QMIs against the Salt and Pepper noise. Tables 4 and 5 are the classification results on the Salt and Pepper noised color objects with different noise density (0.03 and 0.05). The experimental results show that the proposed QMIs are robust to Salt and Pepper noise, and the classification accuracy is better than the CMIs and QZMIs.

3.3.3. Computation complexity of different kinds of invariants

Last, we give a comparison of different moment invariants in the aspect of Computational complexity. In the above experiments, the order of moment invariants (CMIs, QZMIs and QMIs) in the descriptor sets is from 1 to 4. A detailed description of the average computation times of different invariants on the testing image sets (car, cup and bottle image) are listed in Table 6.

The data in the first line of Table 6 are the average computation time for different kinds of invariants on the noise-free car, cup and bottle images. The data from second to fifth line are the average computation time for different kinds of invariants on the noisy corrupted image sets. The data in the last line are the mean values of each column.

From the last line of Table 6 we can see that the average computation time for CMIs were shortest of all, the proposed QMIs were second short and the QZMIs were the most time-consuming. In more detail, the computation of one lower order complex moment invariants for car image needs about 0.0194 s, 0.3239 s for the quaternion Zernike moment invariants, and 0.0640 s for the proposed invariants.

In comparison with the CMIs, the computation time of CMIs approximately 3.3 times faster than the proposed QMIs. However, the CMIs deal with the grayscale image whereas the QMIs deal with the color image. The amount of data for color image is 3 times larger than the grayscale one. In consideration of the quantity of data, the average computation times of the lower order QMIs are similar to the CMIs. Therefore, the proposed QMIs have certain superiority.

In comparison with the QZMIs, the average computation time of lower order QMIs approximately 5 times faster than the QZMIs. This is mainly caused by the following facts. The quaternion Zernike moments are defined in the polar coordinate and the coordinate conversion should be performed for the computation of QZMIs. Besides, the kernel function of quaternion Zernike moments is a set of Zernike polynomials. The realization of QZMIs is much more time-consuming whether the coordinate transformation or the computation of Zernike polynomials. Therefore, the proposed QMIs perform better than the QZMIs in the aspect of computation complexity.

Fig. 3. The image corrupted by different noise. (a1) is the original image; (a2) is the image with gaussian noise (variance = 0.01); (a3) is the image with gaussian noise (0.03); (a4) is the image with Salt and Pepper noise (noise density = 0.03); and (a5) is the image with Salt and Pepper noise (0.05).

Table 2
Classification accuracies (%) of different moment invariants with Gaussian noise (variance = 0.01).

Number of invariants	Average classification accuracy (%)								
	Car images			Cup images			Bottle images		
	CMIs	QZMIs	QMIs	CMIs	QZMIs	QMIs	CMIs	QZMIs	QMIs
5	31.14	60.91	64.46	60.75	83.08	91.26	42.96	76.80	79.76
6	31.07	64.69	69.39	62.54	87.30	94.10	44.01	82.42	85.69
7	30.59	67.05	73.26	64.13	89.85	95.85	43.82	86.23	89.18
8	30.32	68.38	76.36	65.97	92.08	97.79	44.42	88.83	91.36

Table 3
Classification accuracies (%) of different moment invariants with Gaussian noise (variance = 0.03).

Number of invariants	Average classification accuracy (%)								
	Car images			Cup images			Bottle images		
	CMIs	QZMIs	QMIs	CMIs	QZMIs	QMIs	CMIs	QZMIs	QMIs
5	27.80	49.47	58.10	53.09	78.40	86.02	36.70	66.85	69.75
6	27.81	52.29	63.09	53.93	84.03	90.51	37.05	72.10	74.54
7	27.70	54.14	67.11	54.20	87.95	93.13	37.19	76.01	77.66
8	27.01	55.26	70.58	53.64	90.71	94.74	38.31	78.80	79.68

Table 4
Classification accuracies (%) of different moment invariants with Salt and Pepper noise (noise density = 0.03).

Number of invariants	Average classification accuracy (%)								
	Car images			Cup images			Bottle images		
	CMIs	QZMIs	QMIs	CMIs	QZMIs	QMIs	CMIs	QZMIs	QMIs
5	28.17	56.15	60.92	60.29	81.47	90.60	38.07	72.84	79.73
6	28.13	59.75	65.85	62.27	86.25	93.54	38.51	77.29	85.51
7	28.87	62.09	69.66	63.81	89.66	94.98	39.24	80.80	89.32
8	29.55	63.25	73.18	64.29	92.66	95.45	40.78	83.38	92.01

Table 5
Classification accuracies (%) of different moment invariants with Salt and Pepper noise (noise density = 0.05).

Number of invariants	Average classification accuracy (%)								
	Car images			Cup images			Bottle images		
	CMIs	QZMIs	QMIs	CMIs	QZMIs	QMIs	CMIs	QZMIs	QMIs
5	29.85	51.56	53.62	58.48	78.92	87.82	35.99	70.52	73.17
6	29.97	54.76	57.57	61.12	84.23	91.07	36.06	75.30	78.75
7	30.06	56.87	60.62	62.99	88.06	92.61	36.17	78.34	83.07
8	30.06	58.38	62.60	64.48	90.65	93.70	36.49	79.81	85.91

Table 6
Computation times (s) of different moment invariants.

Different image sets	Average computation times (s)								
	Car images			Cup images			Bottle images		
	CMIs	QZMIs	QMIs	CMIs	QZMIs	QMIs	CMIs	QZMIs	QMIs
Noise-free	0.0185	0.3180	0.0622	0.0184	0.3261	0.0641	0.0182	0.3244	0.0642
GN (0.01)	0.0192	0.3236	0.0636	0.0202	0.3268	0.0658	0.0208	0.3292	0.0650
GN (0.03)	0.0197	0.3249	0.0642	0.0211	0.3326	0.0653	0.0210	0.3299	0.0647
S&P (0.03)	0.0198	0.3257	0.0647	0.0203	0.3329	0.0657	0.0203	0.3293	0.0651
S&P (0.05)	0.0201	0.3273	0.0650	0.0206	0.3332	0.0710	0.0204	0.3300	0.0652
Mean	0.0194	0.3239	0.0640	0.0201	0.3303	0.0664	0.0201	0.3285	0.0649

3.3.4. Experiment on the textured color image sets

Texture is an important feature of objects in an image. Texture classification is a fundamental problem in computer vision and pattern recognition tasks [2,57,7,56,31,49,23,21,19,22,29]. The objective of the following experiments is to verify the performance of the proposed QMIs for the textured color image sets. In this experiment, we also investigate the robustness of the proposed QMIs to additive noise. The experiments are carried out on the selected twenty color images, as shown in Fig. 4, from the Vision Texture homepage [34].

With the same method in Subsection 3.2, we obtained the testing and training image sets for color texture classification experiments. From Fig. 4 we are creating altogether 3080 samples as the final testing textured image set, and forming a training set of 100 samples for the SVMs to obtain the related parameters. The classification results using different moment invariants are listed in Table 7. It can be observed from this table that the proposed QMIs work better than the CMIs and the QZMIs in terms of color texture classification.

Next, we present an object classification experiment with more complex scenes. The experiment is carried out on a set of multiple colored objects as shown in Fig. 5, where each image contains four different color textures from the Vision Texture homepage.

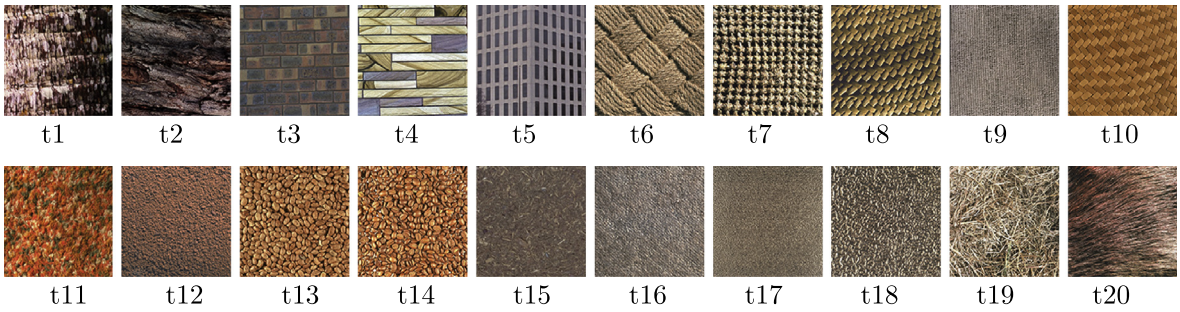

Fig. 4. Twenty images selected from the Vision Texture homepage for color object classification. (t1–t20) are the different textured color images. (For interpretation of the references to color in this figure legend, the reader is referred to the web version of this article.)

Table 7
Classification accuracies (%) of different moment invariants for the textured color objects.

Number of invariants	Average classification accuracy (%)								
	Noise-free			GN (0.01)			S&P (0.03)		
	CMIs	QZMIs	QMIs	CMIs	QZMIs	QMIs	CMIs	QZMIs	QMIs
5	62.04	90.20	92.68	46.92	68.40	69.86	43.44	61.32	64.95
6	65.51	93.81	94.85	49.23	72.69	73.73	45.43	65.30	69.53
7	67.91	95.83	95.61	51.09	75.31	76.43	46.48	68.19	72.37
8	70.06	96.75	96.36	52.40	77.05	78.18	47.24	70.68	73.96

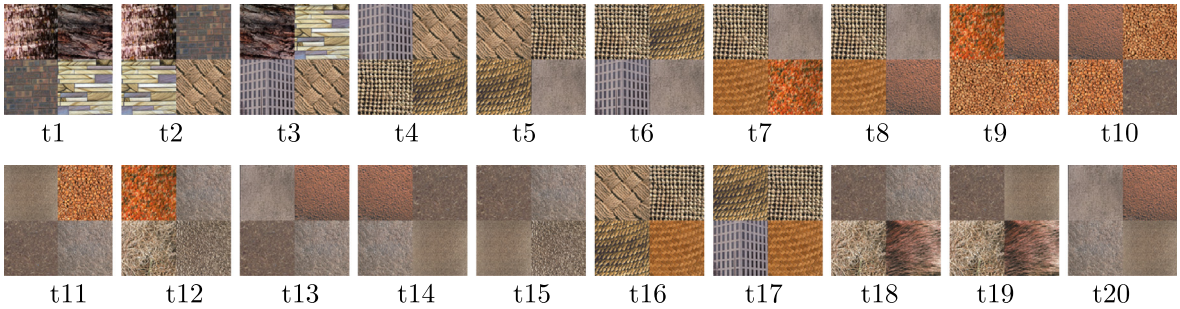

Fig. 5. Twenty images for multiple colored object classification. (For interpretation of the references to color in this figure legend, the reader is referred to the web version of this article.)

Table 8
Accuracies (%) of different moment invariants for multiple colored object classification.

Number of invariants	Average classification accuracy (%)								
	Noise-free			GN (0.01)			S&P (0.03)		
	CMIs	QZMIs	QMIs	CMIs	QZMIs	QMIs	CMIs	QZMIs	QMIs
5	57.06	86.03	92.41	47.87	78.81	84.50	50.36	76.58	80.92
6	60.71	91.08	96.13	50.76	84.64	89.38	53.45	82.31	85.91
7	62.84	93.66	97.82	52.48	87.98	92.44	55.57	85.57	89.10
8	65.06	95.10	98.60	53.83	89.48	94.58	57.08	87.24	91.43

In this multiple colored object classification experiments, the testing and training image sets are generated from Fig. 5. We obtained altogether 3080 samples as the final testing image set, and formed a training set with 100 samples for the SVMs. The robustness of the proposed QMIs to additive noise is also considered in this experiment. The experimental results using different moment invariants for the multiple color objects classification are listed in Table 8. The experimental results show that the proposed QMIs are robust to similarity transform under the conditions of noise-free, Gaussian white noise and

Salt and Pepper noise. It can be observed from Table 8 that the proposed QMIs perform better than the CMIs and the QZMIs in terms of multiple colored texture classification.

The experimental results in the previous subsection show that the proposed QMIs perform best from either classifying the noise-free color images or the noise corrupted images. Although the CMIs have the lowest computation complexity, however, they cannot classify the color objects well. In addition, the average computation times of lower order QMIs are similar as CMIs, and all faster than the QZMIs. In summary, we can arrive at a conclusion that the proposed QMIs are more robust to additive noise and have more discrimination power than the representative moment-based methods proposed in [47,25,15,4].

4. Conclusion and future work

In this study, the quaternion moments for color image are proposed. We show that the quaternion moments are the generalization of traditional complex moments. The advantages of the proposed moments are threefold. First, the proposed moment function are implemented in the Cartesian coordinate, which can not only save more computation time than the quaternion Zernike moments defined in the polar coordinate but also improve the numerical stability; second, it can not only process color image but also grayscale one; Last, it can process color image in a holistic manner, and parallel process R, G, and B components without losing color information.

The similarity invariants based on quaternion moment are constructed for color image. The QMIs combined with the SVMs for color objects classification is investigated in our experiments. The experimental results show that the classification accuracy of the proposed invariants is better than the other competing moment-based methods. The study reveals that the proposed quaternion moment invariants are potentially useful as feature descriptor in the fields of color image processing and object recognition.

The limitation of moment-based invariants is its global property, that is, all the information including background and objects within the image are considered in the calculation. The second experiment in Section 3.3.4 is to verify the classification accuracy of multiple colored objects. However, the computation of moment invariants in this experiment was still from a global perspective. Our future work will be focused on the construction of local moment-based invariants. Besides, the color scene classification using moment-based invariants is also worth studying.

Acknowledgments

We thank Professor S. Honghai for helpful discussion, Dr. J. Wang for improving the linguistic quality. We thank the anonymous referees for their helpful comments and suggestions that improved the quality of this manuscript. Thanks are also extended to the editors for their work. This work was supported by National Basic Research Program of China (973 Program, Grant No. 2009CB72400102A), by National Natural Science Foundation of China (Grant No. 61203242) and by Key Science and Technology Project of Jilin Province (Grant No. 11ZDGG001).

Appendix A

We use left-side, right-side and two-side moment function, respectively, to construct the QMIs descriptor set $\{\Phi(1,0), \Phi(0,1), \Phi(2,0), \Phi(0,2), \Phi(2,1), \Phi(2,2), \Phi(3,0), \Phi(3,1)\}$. Then we compute the above invariants on the testing image set (containing 1540 images). The experimental results are listed in Table 9. The numerical stability of the QMIs were evaluated by the σ/μ index, where σ denotes the standard deviation of the invariants, and μ the mean value. The smaller σ/μ indicates better numerical stability.

Table 9
The σ/μ of the different QMIs for the testing bottle set with 1540 images.

	$\Phi(1,0)$	$\Phi(0,1)$	$\Phi(2,0)$	$\Phi(0,2)$	$\Phi(2,1)$	$\Phi(2,2)$	$\Phi(3,0)$	$\Phi(3,1)$
Left-side	0.1039	0.1048	0.0584	0.0590	0.0401	0.0444	0.0366	0.0369
Right-side	0.1048	0.1039	0.0590	0.0584	0.0395	0.0444	0.0370	0.0382
Two-side	0.1039	0.1039	0.0584	0.0584	0.0405	0.0444	0.0366	0.0384

Table 10
Left-side based QMIs with different unite pure quaternion for the testing set of 1540 images.

	$\Phi(1,0)$	$\Phi(0,1)$	$\Phi(2,0)$	$\Phi(0,2)$	$\Phi(2,1)$	$\Phi(2,2)$	$\Phi(3,0)$	$\Phi(3,1)$
$\mu = i$	0.1034	0.1071	0.0592	0.0580	0.0392	0.0444	0.0357	0.0378
$\mu = j$	0.1062	0.1051	0.0624	0.0565	0.0427	0.0444	0.0388	0.0382
$\mu = k$	0.1064	0.1060	0.0565	0.0640	0.0401	0.0444	0.0357	0.0370
$\mu = (i+j+k)/\sqrt{3}$	0.1039	0.1048	0.0584	0.0590	0.0401	0.0444	0.0366	0.0369

In Table 9, the "$\Phi(\cdot,\cdot)$" in each column is constructed by left-, right-, and two-side moment function, respectively. It can be observed that the σ/μ values are almost unchanged for each column. That is to say, the choices of different types of moment function have little influence on the discrimination power for the QMIs.

In the second experiments, we verified that the choices of different unite pure quaternion cannot significantly influence the discrimination power of the QMIs. We set $\mu = i,\ \mu = j,\ \mu = k$ and $\mu = (i+j+k)/\sqrt{3}$ in the left-side moment function, separately, to compute the QMIs descriptor set. The results can be found in the following table.

We can also find in each column of Table 10 that the σ/μ values are almost unchanged for different "μ". The above two experiments indicate that the discrimination power almost unchanged whether we use different types of moment function or select different unite pure quaternion.

References

[1] T. Ahonen, M. Pietikäinen, Image description using joint distribution of filter bank responses, Pattern Recogn. Lett. 30 (2009) 368–376.
[2] A.R. Backes, D. Casanova, O.M. Bruno, Texture analysis and classification: a complex network-based approach, Inform. Sci. 219 (2013) 168–180.
[3] C.J.C. Burges, A tutorial on support vector machines for pattern recognition, Data Min. Knowl. Disc. 2 (1998) 121–167.
[4] B.J. Chen, H.Z. Shu, H. Zhang, G. Chen, C. Toumoulin, J.L. Dillenseger, L.M. Luo, Quaternion Zernike moments and their invariants for color image analysis and object recognition, Signal Process. 92 (2012) 308–318.
[5] C. Deng, X. Gao, X. Li, D. Tao, A local Tchebichef moments-based robust image watermarking, Signal Process. 89 (2009) 1531–1539.
[6] P. Denis, P. Carre, C.F. Maloigne, Spatial and spectral quaternionic approaches for colour images, Comput. Vis. Image Und. 107 (2007) 74–87.
[7] M. Diker, A.A. Ugur, Textures and covering based rough sets, Inform. Sci. 184 (2012) 44–63.
[8] T.A. Ell, S.J. Sangwine, Hypercomplex fourier transforms of color images, IEEE Trans. Image Proc. 16 (2007) 22–35.
[9] J. Flusser, On the independence of rotation moment invariants, Pattern Recognit. 33 (2000) 1405–1410.
[10] J. Flusser, J. Kautsky, F. Šroubek, Implicit moment invariants, Int. J. Comput. Vis. 86 (2010) 72–86.
[11] V. Franc, V. Hlaváč, Statistical Pattern Recognition Toolbox for Matlab, Center for Machine Perception, Czech Technical University, 2011 <http://www.cmp.felk.cvut.cz/cmp/software/stprtool>.
[12] A. Gepperth, B. Mersch, J. Fritsch, C. Goerick, Color object recognition in real-world scenes, LNCS 4669 (2007) 583–592.
[13] F. Ghorbel, S. Derrode, R. Mezhoud, T. Bannour, S. Dhahbi, Image reconstruction from a complete set of similarity invariants extracted from complex moments, Pattern Recognit. Lett. 27 (2006) 1361–1369.
[14] L. Guo, M. Dai, M. Zhu, Multifocus color image fusion based on quaternion curvelet transform, Opt. Exp. (2012) 18846–18860.
[15] L. Guo, M. Zhu, Quaternion Fourier–Mellin moments for color images, Pattern Recognit. 44 (2011) 187–195.
[16] L. Guo, M. Zhu, X. Ge, Reduced biquaternion canonical transform, convolution and correlation, Signal Process. 91 (2011) 2147–2153.
[17] M.K. Hu, Visual pattern recognition by moment invariants, IRE Trans. Inf. Theor. 8 (1962) 179–187.
[18] Y. Huang, K. Huang, D. Tao, T. Tan, X. Li, Enhanced biologically inspired model for object recognition, IEEE Trans. Syst., Man, Cybern., Part B 41 (2011) 1668–1680.
[19] J.J.M.S. Junior, A.R. Backes, P.C. Cortez, Texture analysis and classification using shortest paths in graphs, Pattern Recognit. Lett. 34 (2013) 1314–1319.
[20] C.L. Lim, B. Honarvar, K.H. Thung, R. Paramesran, Fast computation of exact zernike moments using cascaded digital filters, Inform. Sci. 181 (2011) 3638–3651.
[21] L. Liu, L. Zhao, Y. Long, G. Kuang, P. Fieguth, Extended local binary patterns for texture classification, Image Vis. Comput. 30 (2012) 86–99.
[22] O. Losson, A. Porebski, N. Vandenbroucke, L. Macaire, Color texture analysis using CFA chromatic co-occurrence matrices, Comput. Vis. Image Und. 117 (2013) 747–763.
[23] R. Maani, S. Kalra, Y.H. Yang, Noise robust rotation invariant features for texture classification, Pattern Recognit. 46 (2013) 2103–2116.
[24] H.J.A. Martn, M. Santos, J. de Lope, Orthogonal variant moments features in image analysis, Inform. Sci. 180 (2010) 846–860.
[25] F. Mindru, T. Tuytelaars, L.V. Gool, T. Moons, Moment invariants for recognition under changing viewpoint and illumination, Comput. Vis. Image Und. 94 (2004) 3–27.
[26] Y.S.A. Mostafa, D. Psaltis, Recognitive aspects of moment invariants, IEEE Trans. Pattern Anal. Mach. Intell. 6 (1984) 698–706.
[27] Y.S.A. Mostafa, D. Psaltis, Image normalization by complex moments, IEEE Trans. Pattern Anal. Mach. Intell. 7 (1985) 46–55.
[28] R. Mukundan, S.H. Ong, P.A. Lee, Image analysis by Tchebichef moments, IEEE Trans. Image Process. 10 (2001) 1357–1364.
[29] L. Nanni, A. Lumini, S. Brahnam, Survey on lbp based texture descriptors for image classification, Exp. Syst. Appl. 39 (2012) 3634–3641.
[30] S.A. Nene, S.K. Nayar, H. Murase, The Columbia University Image Library Database (Coil-100 Color Images), 1996 <http://www.cs.columbia.edu/CAVE/software/softlib/coil-100.php>.
[31] M.D.R. Ortega, L. Ortega, F.R. Feito, A new approach to create textured urban models through genetic algorithms, Inform. Sci. 243 (2013) 1–19.
[32] G.A. Papakostasa, E.G. Karakasisb, D.E. Koulouriotisb, Novel moment invariants for improved classification performance in computer vision applications, Pattern Recognit. 43 (2010) 58–68.
[33] S.C. Pei, C.M. Cheng, Efficient implementation of quaternion fourier transform, convolution, and correlation by 2-D complex FFT, IEEE Trans. Signal Process. 49 (2001) 2783–2797.
[34] R. Picard, C. Graczyk, S. Mann, J. Wachman, L. Picard, L. Campbell, Vision Texture Homepage, 2002 <http://vismod.media.mit.edu/vismod/imagery/VisionTexture/vistex.html>.
[35] J.M. Pozo, M.C. Villa-Uriol, A.F. Frangi, Efficient 3D geometric and zernike moments computation from unstructured surface meshes, IEEE Trans. Pattern Anal. Mach. Intell. 33 (2011) 471–484.
[36] E. Rahtu, T. Heikkilä, V. Ojansivu, T. Ahonen, Local phase quantization for blur-insensitive image analysis, Image Vis. Comput. 30 (2012) 501–512.
[37] S.J. Sangwine, Fourier transforms of color images using quaternion or hypercomplex numbers, Electron. Lett. 32 (1996) 1979–1980.
[38] S.J. Sangwine, N.L. Bihan, Quaternion polar representation with a complex modulus and complex argument inspired by the Cayley–Dickson form, Adv. Appl. Clifford Algebras 20 (2010) 111–120.
[39] S.J. Sangwine, T.A. Ell, N.L. Bihan, Fundamental representations and algebraic properties of biquaternions or complexified quaternions, Adv. Appl. Clifford Algebras 21 (2011) 607–636.
[40] B. Schölkopf, A.J. Smola, Learning with Kernels: Support Vector Machines, Regularization, Optimization, and Beyond, MIT Press, 2001.
[41] Y. Sheng, H.H. Arsenault, Experiments on pattern recognition using invariant Fourier–Mellin descriptors, J. Opt. Soc. Am. A 3 (1986) 771–776.
[42] Y. Sheng, J. Duvernoy, Circular-Fourier-radial-Mellin transform descriptors for pattern recognition, J. Opt. Soc. Am. A 3 (1986) 885–888.
[43] L. Shi, B. Funt, Quaternion color texture segmentation, Comput. Vis. Image Und. 107 (2007) 88–96.
[44] C. Singh, E. Walia, R. Upneja, Accurate calculation of Zernike moments, Inform. Sci. 233 (2013) 255–275.
[45] D. Song, D. Tao, Biologically inspired feature manifold for scene classification, IEEE Trans. Image Process. 19 (2010) 174–184.
[46] O.N. Subakan, B.C. Vemuri, A quaternion framework for color image smoothing and segmentation, Int. J. Comput. Vis. 91 (2011) 233–250.
[47] T. Suk, J. Flusser, Affine moment invariants of color images, in: Proceedings of 13th International Conference on Computer Analysis of Images and Patterns (CAIP2009), 2009, pp. 334–341.
[48] T. Suk, J. Flusser, Affine moment invariants generated by graph method, Pattern Recognit. 44 (2011) 2047–2056.
[49] X. Sun, J. Wang, M.F. She, L. Kong, Scale invariant texture classification via sparse representation, Neurocomputing 122 (2013) 338–348.

[50] J.W. Tanaka, L.M. Presnell, Color diagnosticity in object recognition, Percept. Psychophys. 61 (1999) 1140–1153.
[51] M.R. Teague, Image analysis via the general theory of moments, J. Opt. Soc. Am. 70 (1980) 920–930.
[52] V.N. Vapnik, The Nature of Statistical Learning Theory, second ed., Springer-Verlag, NewYork, 2000.
[53] P.T. Yap, R. Paramesran, S.H. Ong, Image analysis by Krawtchouk moments, IEEE Trans. Image Procss. 12 (2003) 1367–1377.
[54] P.T. Yap, R. Paramesran, S.H. Ong, Image analysis using hahn moments, IEEE Trans. Pattern Anal. Mach. Intell. 29 (2007) 2057–2062.
[55] W. Yuanbin, Z. Bin, Y. Tianshun, Projective invariants of co-moments of 2D images, Pattern Recognit. 43 (2010) 3233–3242.
[56] B. Zhang, X. Wang, F. Karray, Z. Yang, D. Zhang, Computerized facial diagnosis using both color and texture features, Inform. Sci. 221 (2013) 49–59.
[57] C. Zhu, R. Wang, Local multiple patterns based multiresolution gray-scale and rotation invariant texture classification, Inform. Sci. 187 (2012) 93–108.